Effective enhancement of gas separation performance in mixed matrix membranes using core/shell structured multi-walled carbon nanotube/graphene oxide nanoribbons

Xue, Qingzhong; Pan, Xinglong; Li, Xiaofang; Zhang, Jianqiang; Guo, Qikai

[Link to publication in University of Groningen/UMCG research database](#)

Effective enhancement of gas separation performance in mixed matrix membranes using core/shell structured multi-walled carbon nanotube/graphene oxide nanoribbons

Qingzhong Xue[1,2], Xinglong Pan[1,2], Xiaofang Li[2], Jianqiang Zhang[2] and Qikai Guo[3]

[1] State Key Laboratory of Heavy Oil Processing, China University of Petroleum, People's Republic of China
[2] College of Science, China University of Petroleum, People's Republic of China
[3] Zernike institute of advanced materials, University of Groningen, The Netherlands

E-mail: xueqingzhong@tsinghua.org.cn

Abstract

Novel core/shell structured multi-walled carbon nanotube/graphene oxide nanoribbons (MWCNT@GONRs) nanohybrids were successfully prepared using a modified chemical longitudinal unzipping method. Subsequently, the MWCNT@GONRs nanohybrids were used as fillers to enhance the gas separation performance of polyimide based mixed matrix membranes (MMMs). It is found that MMMs concurrently exhibited higher gas selectivity and higher gas permeability compared to pristine polyimide. The high gas selectivity could be attributed to the GONRs shell, which provided a selective barrier and large gas adsorbed area, while the high gas permeability resulted from the hollow structured MWCNTs core with smooth internal surface, which acted as a rapid transport channel. MWCNT@GONRs could be promising candidates to improve gas separation performance of MMMs due to the unique microstructures, ease of synthesis and low filling loading.

S Online supplementary data available from stacks.iop.org/NANO/28/065702/mmedia

Keywords: MWCNT@GONRs, normalized selectivity, selective barrier, transport channel, core/shell structure

(Some figures may appear in colour only in the online journal)

1. Introduction

Membrane technology has drawn significant attention on gas separation due to its inherent advantages such as higher efficiency, lower cost and simplicity, compared with conventional separation technologies (cryogenic separation and pressure swing adsorption). However, the commercialization of membranes for gas separation is limited [1–4]. The major reason is the existence of trade-off trend between gas permeability and selectivity, as shown in the upper bound relationship by Robeson [5, 6]. In order to surpass the upper bound correlation, mixed matrix membranes (MMMs), comprising of dispersed filler (e.g., zeolite [7–9], metal organic frameworks [10–12], carbon nanotubes (CNTs) [13–16] and graphene oxide (GO) [17–20]) were fabricated as promising candidates [21–23].

Among these fillers, CNTs have become a focal point for gas separation because of their unique properties, such as

nano-sized hollow structure, smooth internal surface, excellent mechanical and thermal properties [24, 25]. For one thing, the nano-sized hollow structure and smooth internal surface of CNTs promote the rapid transportation of gas molecules through them [26–30]. For example, Skoulidas *et al* reported the gas permeation rates in CNTs are 3–4 orders of magnitude higher than that in ZSM-12 and silicalite due to the inherent smoothness of CNTs [31]. For another thing, the excellent mechanical and thermal properties of CNTs can also significantly enhance the mechanical strength and thermostability of polymer matrix [15, 32]. All these features are beneficial for the enhancement of gas separation performance of MMMs. Unfortunately, the aggregation of pristine CNTs and the bad compatibility between CNTs and polymer are major hurdle to efficiently fabricate MMMs and enhance permeability and selectivity simultaneously [33–35].

GO is a novel two-dimensional material with a large amount of oxygen-containing groups including epoxide, hydroxyl and carboxylic acid group on their basal planes and edges [36–40]. The huge specific surface area and oxidized functional groups of GO can selectively absorb abundant gas molecules to improve the solubility coefficients of MMMs. For instance, Shan *et al* reported that the effects of groups on the CO_2 adsorption ability of graphene were as follows: $-OH > -COOH > -NH_2 > -CH_3$, which was ascribed to the different polarities and sizes of the functional groups. And $-OH$, $-COOH$ and $-NH_2$ were more polar than CH_3, so they had a stronger interaction with CO_2 molecules [38]. Meanwhile, when GO oriented horizontally in polymer matrix, they could be acted as a better barrier to improve gas selectivity [41–43]. Kim *et al* revealed that different gas had different effective diffusion pathway between the GO interlayers and the gas permeance order was $CO_2 > H_2 > He > CH_4 > O_2 > N_2$ at 298 K [42]. Furthermore, GO can be dispersed easily in polar solvent such as N, N-dimethylformamide (DMF), N, N-dimethylacetamide (DMAc) and N-Methyl-2-pyrrolidone (NMP) to fabricate homogeneous MMMs. However, GO prone to wrinkle when they are dispersed individually in polymer matrix, so gas permeability of MMMs will decrease obviously at certain concentrations of GO due to the barrier of GO [44–46].

As mentioned before, CNTs could effectively enhance gas permeability and GO could enhance gas selectivity, respectively. Hence, incorporating CNTs and GO in MMMs may be a fantastic design to synchronously enhance gas permeability and selectivity. Wu *et al* reported that mixing 10 wt% of CNTs and GO into MMMs enhanced the gas separation performance for CO_2/N_2 and CO_2/CH_4 compared with that of MMMs adding individual CNTs or GO [46]. However, the high loadings of CNTs and GO mixture were simply mixed by sonicating. The aggregation of pristine CNTs, the bad compatibility between CNTs and polymer matrix and massive wrinkles of GO could not be averted in MMMs.

In this paper, the novel core/shell structured multi-walled CNT/GO nanoribbons (MWCNT@GONRs) were fabricated by simple method. Compared with aforementioned fillers, MWCNT@GONRs nanohybrids effectively solved the hurdle

of CNTs and GO since the dispersible GONRs shell was in favor of dispersibility of MWCNT@GONRs and the firm MWCNTs core could avoid the wrinkle of GO. And a low loading of MWCNT@GONRs nanohybrids were used as fillers to effectively enhance gas separation performance of MMMs. In addition, the microstructure, thermostability and crystalline characteristic of the nanofillers and MMMs were studied in detail.

2. Experimental section

2.1. Materials

Polyimide (PI) resin powder (Mw = 44 000 g mol^{-1}) was supplied by Alfa Aesar. MWCNTs (purity $\geqslant$ 95 wt%, diameter: 8–20 nm, length 5–15 μm,) and Dimethylacetamide (DMAc) used as solvent were purchased from Aladdin Chemistry Co., Ltd The remaining chemicals were purchased from Sinopharm Chemical Reagent Co., Ltd All reagents were of analytical grade and used without further purification.

2.2. Preparation of MWCNT@GONRs

MWCNT@GONRs were prepared by a modified chemical longitudinal unzipping method of MWCNTs, as previously reported [47, 48]. Typically, MWCNTs (500 mg) were dispersed in a mixture of concentrated H_2SO_4 and concentrated HNO_3 in ratio of 3:1. And the reaction mixture was heated at 333 K for 2 h. Then the product was filtered over a 0.45 μm pore size polytetrafluoroethylene membrane and dried in a vacuum at 318 K to get oxidized MWCNTs powder.

The oxidized MWCNTs (150 mg) were dispersed in concentrated H_2SO_4 (36 ml) under ultrasonication for a few minutes to form a stable suspension. Then H_3PO_4 (85%, 4 ml) was added to the suspension with stirring. And $KMnO_4$ (500 mg) was added slowly with strong stirring. After 1.5 h, the mixture was heated at 333 K for 2 h and then cooled to room temperature. Then the mixture was poured on 100 ml of ice containing H_2O_2 (30%, 5 ml). The product was filtered and washed twice with HCl (20%) to remove metal ions before dispersing in HCl aqueous solution (100 ml, 12%). Afterwards, the mixture was precipitated overnight and the sediment was washed with deionized water several times. Finally, the remaining solid was freeze-dried in a lyophilizer and then MWCNT@GONRs with a certain oxidation degree were obtained.

2.3. Membrane preparation

Dense PI membranes were fabricated by solution-casting method. Prior to membrane fabrication, the PI resin powder and nanofillers (MWCNT@GONRs) were dried at 333 K in a vacuum oven for 24 h to remove the residual moisture. Firstly, the nanofillers were dispersed in DMAc to form stable suspension under mild ultrasonication. The nanofiller concentrations of MMMs were in the range of 0–2 wt%. Then PI resin powder (0.74 g) was added into the suspension, which was stirred vigorously until the mixture formed a

homogeneous suspension. The mixture was left at room temperature for 12 h to remove air bubbles. The resulting solution was cast onto a flat glass at 298 K in DMAc atmosphere for 24 h. Finally, the formed film was left in a vacuum oven at 393 K for 24 h to remove the residual solvent. The pristine PI membrane was also prepared by exactly the same procedure without addition of nanofillers for comparison. The average thickness of resulting membranes was about 20 μm, as measured by a digital micrometer screw gauge.

2.4. Characterization

The surface morphology of MWCNT@GONRs was analyzed by a transmission electron microscope (TEM, JEOL, Japan) at an accelerating voltage of 200 kV. The N_2 adsorption-desorption isotherm of MWCNT@GONRs were measured at 77 K using a surface area and porosity analyzer in order to determine the Brunauer–Emmett–Teller surface areas. Prior to the measurement, MWCNT@GONRs were pretreated under N_2 flow at 573 K. The thermostability of MWCNT@GONRs and membranes were measured using Mettler Toledo thermal gravity analyseis (TGA) instrument from room temperature to 1173 K under nitrogen flow at a heating rate of 10 K min^{-1}. The crystalline properties of membranes were evaluated using x-ray diffraction (XRD) with Cu Kα monochromatized radiation ($\lambda = 1.54$ Å) and operated at 45 kV and 40 mA. The cross-section of membranes was characterized using a field emission scanning electron microscope. All membranes were fractured using liquid nitrogen before scanning.

2.5. Gas permeation measurements

The gas permeabilities of samples were measured by permeation measurement equipment described in the previous literature [49]. The experiments were carried out using the constant volume method and the permeabilities were calculated by the equation (1):

$$P = \frac{273}{76} \times \frac{Vl}{AT\Delta p} \times \left(\frac{\mathrm{d}p}{\mathrm{d}t}\right), \tag{1}$$

where V is the downstream volume (cm^3) at standard temperature and pressure, l is the thickness of membranes (cm), A is the effective area of membranes and Δp is the pressure difference between the feed side and permeate side (cmHg).

The selectivity (α_{ij}) is calculated by the following equation:

$$\alpha_{ij} = \frac{P_i}{P_j} = \frac{D_i}{D_j} \times \frac{S_i}{S_j}. \tag{2}$$

3. Results and discussion

3.1. Characterization of MWCNT@GONRs nanohybrids

The TEM images of MWCNTs and MWCNT@GONRs nanohybrids were shown in figure 1. As shown in figures 1(a)

and (b), the pristine MWCNT showed smooth surfaces and the diameters were distributed from 8–20 nm. And MWCNTs were wrapped by GONRs to form the core/shell structure of MWCNT@GONRs nanohybrids in figures 1(c) and (d). The results showed that the length of MWCNT@GONRs nanohybrids was shorter than that of MWCNTs and the aggregation of MWCNTs was solved. Almost all of MWCNTs was oxidized to form MWCNT@GONRs. However, the mass ratios of GONRs in MWCNT@GONRs were different because MWCNTs with thick diameter were oxidized easily.
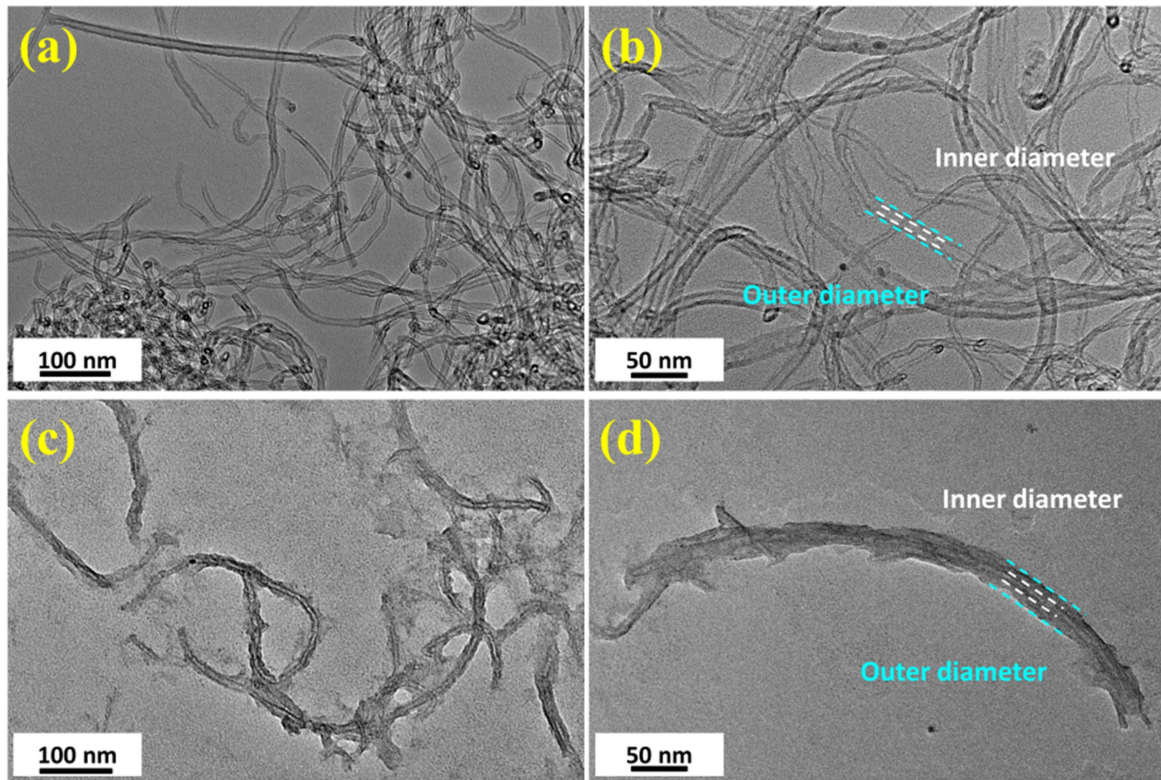
The FTIR spectrum of pristine MWCNTs and core/shell structured MWCNT@GONRs nanohybrids were showed in figure 2. The peaks in spectrum at 3425, 1631 and 1226 cm^{-1} were attributed to the stretching vibration of the C–OH groups, C=O groups and C–O groups, respectively. Accordingly, pristine MWCNTs and MWCNT@GONRs exhibited the same oxygen-containing groups including carboxyl and hydroxyl groups. The oxidation functional groups of pristine MWCNTs may be generated by pretreatment of purification before selling.

Raman spectroscopy was performed in the range of 1000 -2000 cm^{-1} to check the degree of oxidation using an excitation wavelength of 514.5 nm, as shown in figure 3. The Raman spectrum of pristine MWCNTs was shown in figure S1. The two peaks in spectrum were observed at 1355 and 1592 cm^{-1}, indicating the stretching modes of the D band and G band, respectively. The D-band arises from the multiple phonon scattering of defects. The G band arises from the stretching of corresponds to sp^2 hybridization and conjugated double bonds during the formation of the aryl-nanotube bonds. The intensity ratio of the D and G peaks and the variation of their intensity are commonly used to quantify the structural quality of carbon materials [35]. After fitting by mixing a Lorentz shape, it can be found that the intensity ratio of I_D/I_G in MWCNT@GONRs nanohybrids is 0.95, which is similar to GO as reported [50, 51]. Thus, MWCNT@GONRs nanohybrids also possessed a high degree of oxidation.

3.2. Membrane characterization

The cross-section of pristine PI membrane and MMMs with 1 and 2 wt% filler loadings were shown in figure 4. As shown in figures 4(b) and (e), the MWCNT@GONRs were homogeneously dispersed in MMMs due to superior dispersity of GONRs, which was in favor of forming uniform MMMs. Unfortunately, the MWCNT@GONRs agglomerates were found due to their large surface energy and high loadings, as shown in figures 4(c) and (f), which caused the lower selectivity and higher permeability of MMM with 2 wt% filler loading. (The cross-section SEM images of all resultant membranes were shown in figure S2.)

Figure 5 showed the TGA curves of MMMs with different loadings, which indicated the effect of nanofillers on the thermal stability of MMMs. (The TGA curve of MWCNT@GONRs was showed in figure S3.) The TGA curves of the MMMs had two similar weight loss stages. The first weight loss stage in the temperature range of 440–550 K was attributed to the release of physically adsorbed water
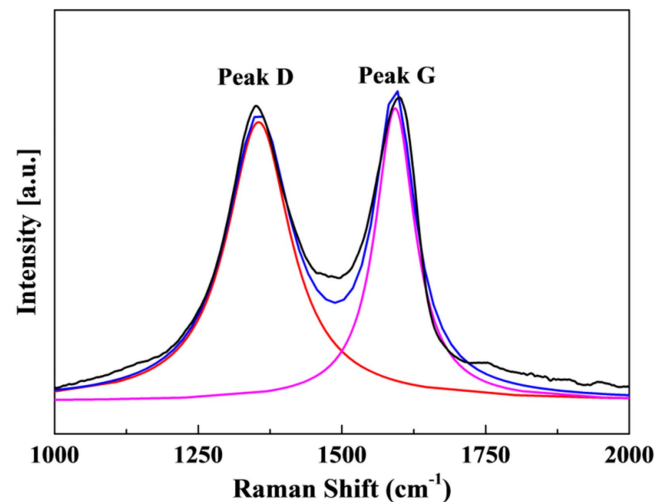
Figure 1. TEM images of pristine MWCNTs (a) and (b) and MWCNT@GONRs nanohybrids (c) and (d).
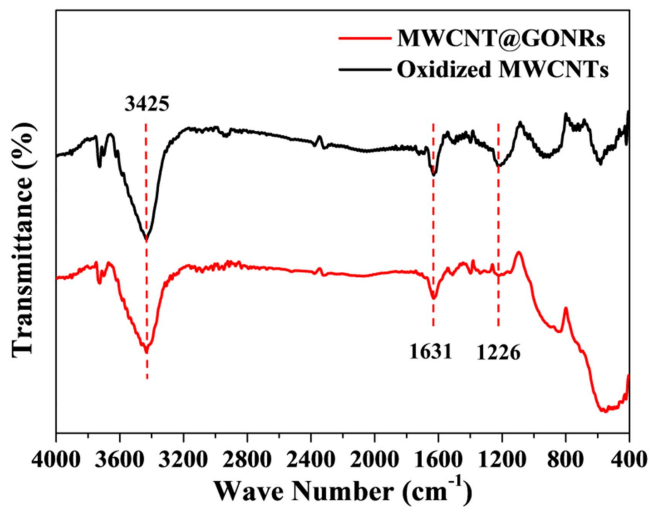

Figure 2. The FTIR spectrum of pristine MWCNTs and core/shell structured MWCNT@GONRs nanohybrids.

Figure 3. Raman spectrum of MWCNT@GONRs nanohybrids.

contained in the samples and decomposition of a part of oxygen-containing groups of nanofillers [52, 53]. And the second stage was mainly caused by the decomposition of polymer main chains [44]. Compared to pristine PI membrane, MMMs showed the higher decomposition temperature and lower water adsorption due to the competitive adsorption of water molecular and nanofillers on polymer chains, which indicated that the interactions of hydrogen bonds between nanofillers and polymer chains was stronger than that between water molecular and polymer chains.

In order to investigate the influence of nanofillers on arrangement of polymer chain, the crystalline structure of MMMs was studied by XRD. The XRD patterns of MMMs were shown in figure 6. The pristine PI membrane is a semicrystalline polymer with diffraction peaks at 16° and 22.6° of 2θ. For PI/MWCNT@GONRs MMMs, the intensity of diffraction peaks decreased and then increased with adding of nanofillers and the intensity of peaks reached to minimum at 1 wt% loading of MWCNT@GONRs, which meant that the crystallinity was destroyed and the degree of crystallinity become lower due to the strong interaction between oxygen containing functional groups of nanofillers and N atom of PI
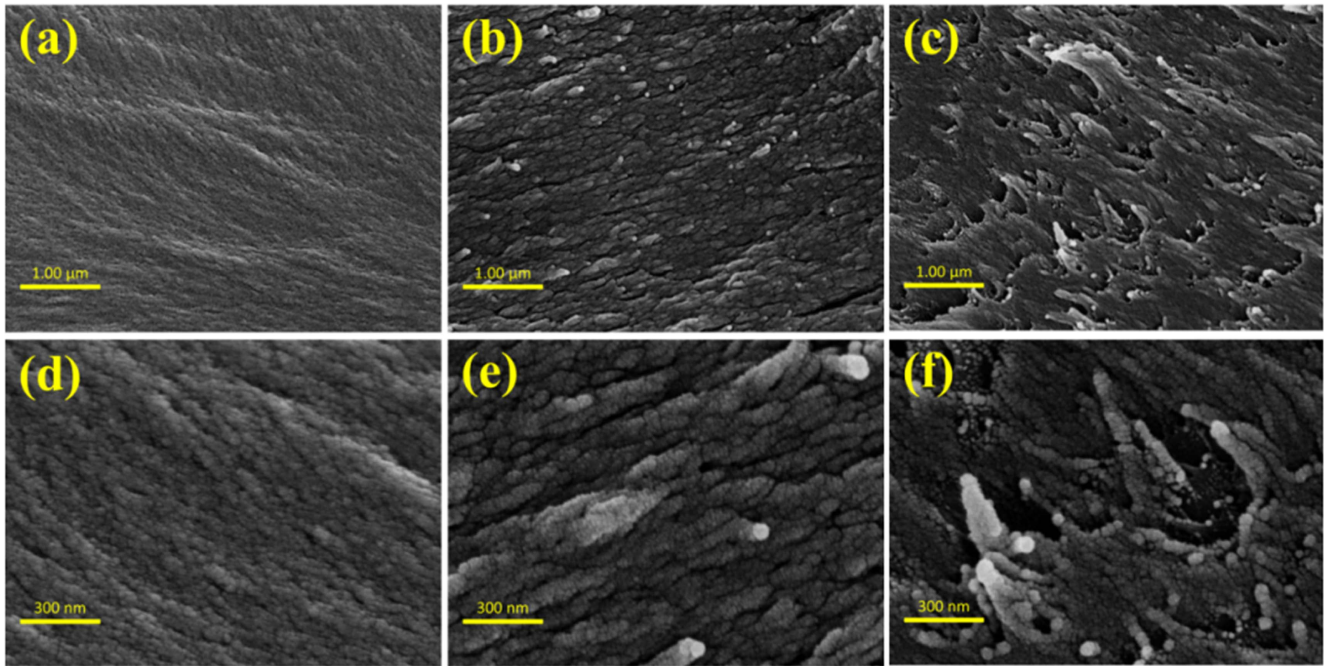
Figure 4. SEM images of the pristine PI membrane (a) and (d) and MMMs at 1 wt% filler loading (b) and (e) and 2 wt% filler loading (c) and (f).
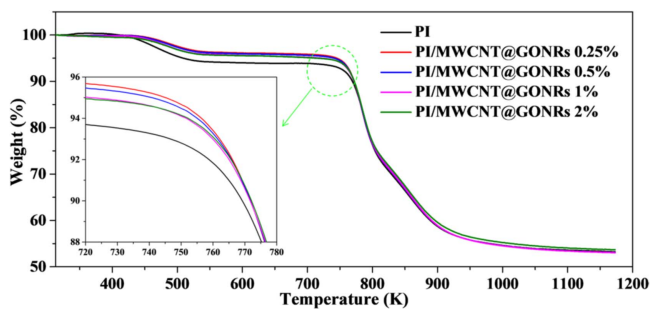
Figure 5. The TGA curves of pure PI membrane and MMMs with different loadings.
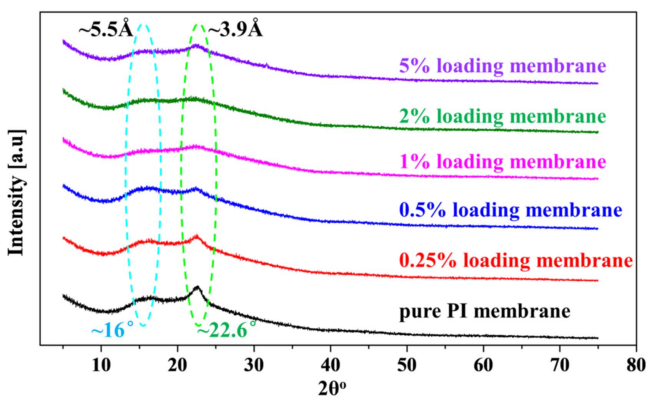
Figure 6. XRD patterns of pure PI membrane and MMMs with different loadings.

chains [15]. Meanwhile, the results implied the better compatibility between nanofillers and PI and dispersibility of MWCNT@GONRs in polymer matrix at 1 wt% loading.

3.3. Separation performance of membranes

The performances of both the MMMs and the reference pristine PI membrane were tested for the separation of H_2, CO_2, N_2 and CH_4 at 35 °C. All values in figures 7(a) and (b) were found to be accurate within 5% error margin, confirming the consistency of both the optimized synthesis procedure and testing method used to evaluate gas separation. The selectivity value of the unfilled reference membrane was lower than already reported results [54], which might be attributed to the smaller molecular weight and different membrane synthesis procedure. But the gas permeability value of the unfilled reference membrane was higher than already reported results [44, 54]. The permeability of H_2 was measured to comparatively study the gas permeation mechanism of membranes due to smaller dynamic diameter of H_2 and weaker interaction between polymer matrix and H_2. In figure 7, the permeability of H_2 was higher than those permeabilities of other gases due to H_2 molecular show smaller dynamic diameter (0.29 nm) and the dynamic diameters of CO_2, N_2 and CH_4 were 0.34, 0.36 and 0.38 nm, respectively. The MMMs showed higher permeability of CO_2 due to the strong interaction between CO_2 and negatively polarized N atoms in polymer chains [38], which was in favor of CO_2 permeability.

With increasing filler loading, the H_2 and CO_2 permeabilities and selectivities increased gradually because of more free volume cavities and stronger interaction between CO_2 and polymer chains [44]. At 0.5 wt% filler loading, the
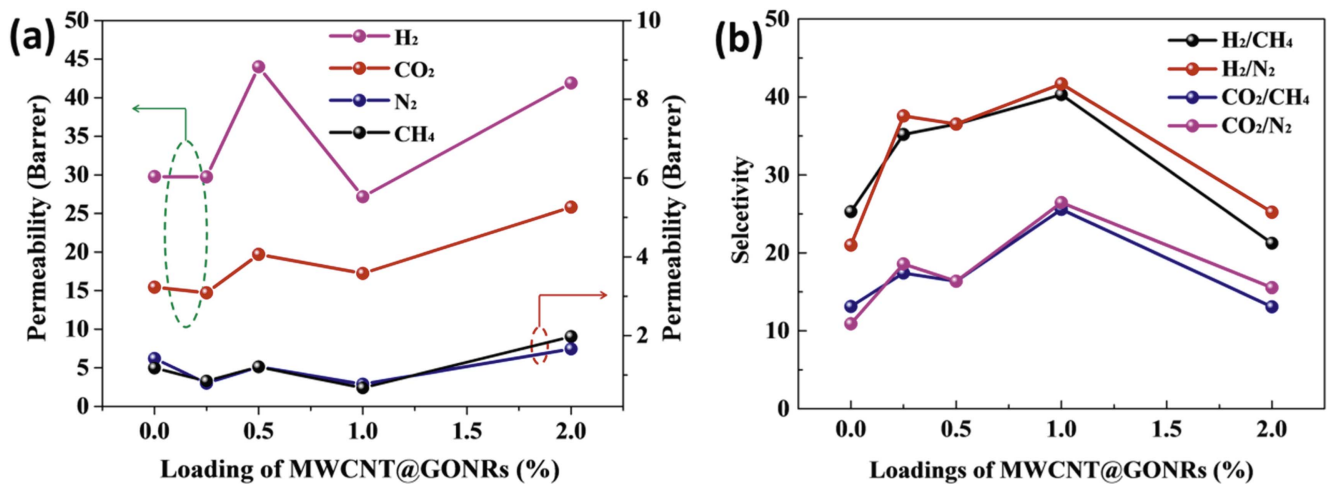
Figure 7. Gas permeabilities (a) and gas selectivities (b) of MMMs with different filler loadings (1 bar and 35 °C).
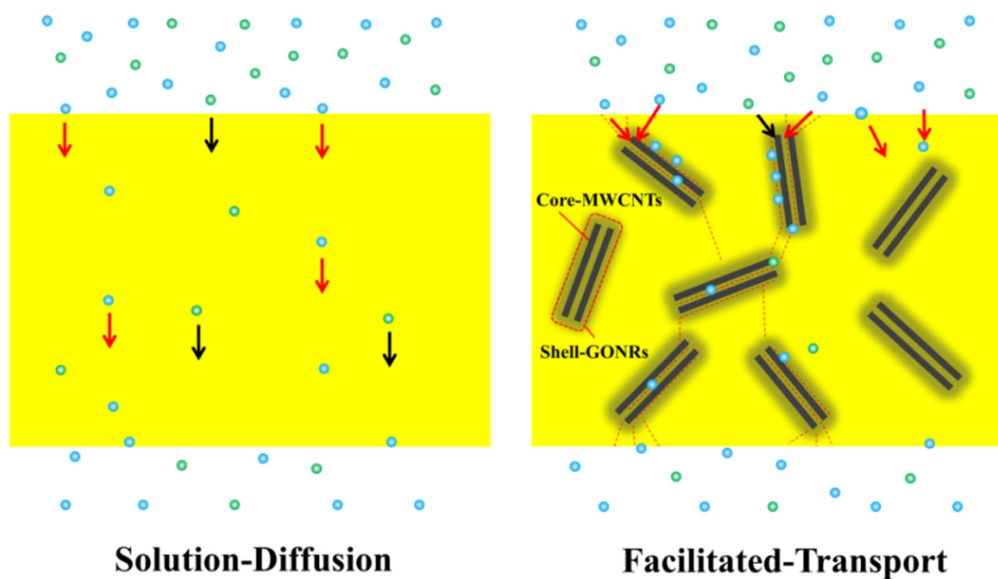

Figure 8. The schematic diagram of gas transport modes in pristine PI membrane and MMMs.

permeabilities of H_2 and CO_2 increased to 148% and 128% and the selectivities of H_2/N_2, H_2/CH_4, CO_2/N_2 and CO_2/CH_4 increased to 174%, 144%, 150% and 125%, respectively. The curve showed a special point at 1 wt% filler loading and gas permeability of H_2 decreased suddenly, which might be caused by the better stretch of GONRs as a barrier layer [45]. But the permeability of CO_2 slightly decreased due to the synergistic effect of smaller longitudinal radius and strong quadrupole moment. The permeabilities of N_2 and CH_4 decreased due to their large dynamic diameter. Thus the selectivities of H_2/N_2, H_2/CH_4, CO_2/N_2 and CO_2/CH_4 increased to 198%, 159%, 243% and 195%, respectively. The MWCNT@GONRs in MMMs began to aggregate when the filler loadings reached 2 wt% so that the permeability increases and selectivity decreased in figures 8(a) and (b).

The schematic diagram of gas transport modes in pristine PI membrane and MMMs were shown in figure 8 and the gas transfer path was marked. The separation mechanism of

pristine PI membrane was solution-diffusion and the separation mechanism of MMMs was facilitated-transport. The effective carrier of this facilitated-transport mechanism was the carboxylate group (–COO^-), which could be contributed by the GONRs shell. CO_2 reacted with –COO^- and free water molecular to produce HCO_3^- as shown in equation (3), and then diffused through the membranes in the form of HCO_3^- ions [55].

$$CO_2 + -COO^- + H_2O \Leftrightarrow -COOH + HCO_3^-. \qquad (3)$$
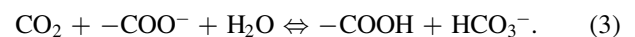
In MMMs, the higher gas selectivity could be attributed to the GONRs shell, which provided a selective barrier and large gas adsorbed area, while the higher gas permeability resulted from the hollow structured MWCNT core with smooth internal surface, which acted as rapid transport channels. At 1 wt% filler loading, the gas permeability of MMMs had a somewhat decrease, but the decrease value was smaller than the reported value of MMMs with GO [17, 45, 46]. The results indicated that the rapid transport
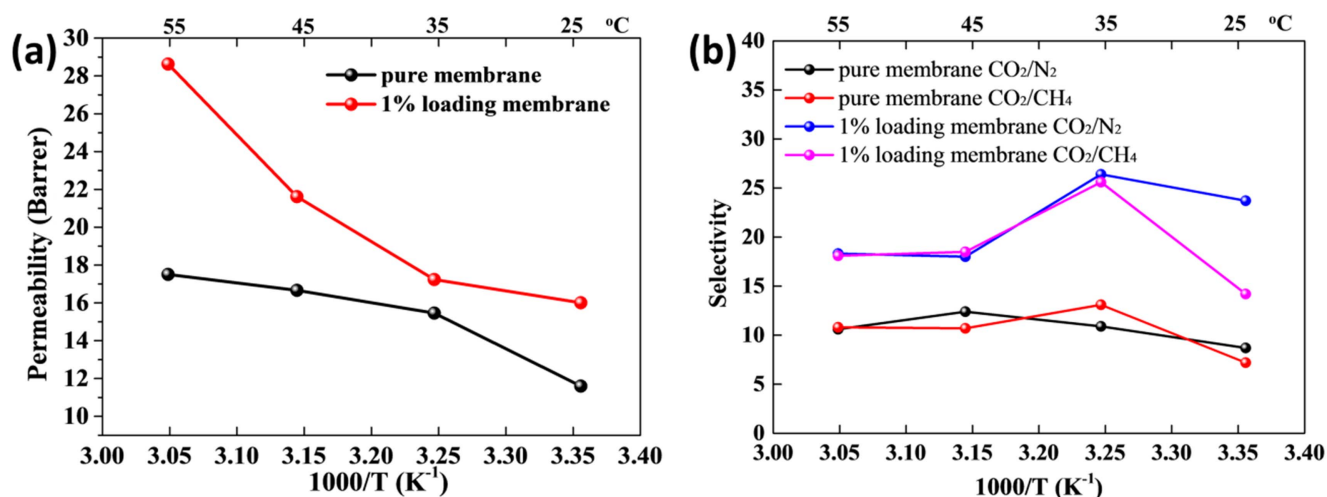
Figure 9. Effect of temperature on CO_2 permeability (a) and selectivity (b) of membranes.

channels of MWCNTs retarded the barrier effect of GONRs to some extent. Therefore, the adding of nanofiller may affect gas permeation by the following means [15, 38, 34, 46]: (a) the functional group at the surface of nanofiller may interact with some gases (CO_2 and CH_4), which enhances the solubility of MMMs; (b) the interaction between polymer chains and nanofiller may enhance gas diffusion in MMMs by increasing the free volumes and disturbing the polymer chains packing; (c) the increased tortuosity for diffusion and the barrier of nanofiller may cause the gas diffusion decrease in MMMs; (d) the agglomeration of nanofiller may enhance the gas diffusion and deteriorate the gas separation performance.

3.4. Effect of operating temperature on membrane performance

In order to study effect of operating temperature on membrane performance, the temperature dependence of CO_2 permeation performance was carried out by varying the operating temperature as shown in figure 10(a). The CO_2 permeability of MMMs with 1 wt% filler loading showed an increase up to 79% as the temperature increased from 25 °C to 55 °C. The kinetic energy of gas molecules increased and the relaxation of the polymeric chains increased with increasing feed temperature, which lowered the activation energy required for gas permeation and enhanced the gas permeability. In order to further study the role of temperature in altering the membrane performance, the activation energy of gas permeation (E_p) was calculated by Arrhenius equation (4) as follow:

$$P = P_0 \exp\left(-\frac{E_P}{RT}\right),\tag{4}$$

where P is the gas permeability, P_0 is the pre-exponential factor, R is the gas constant (8.314 J mol^{-1} K^{-1}) and T is the absolute temperature (K).

The results showed that E_p of MMM with 1 wt% filler loading is 17.4 kJ mol^{-1}, which was lower than that of the previously studied membranes [55]. This was attributed to the increased porosity of membrane imparted by the fillers and

this result supported the argument that the MWCNT@GONRs provided shorter and faster path.

The effect of temperature on CO_2 selectivity of membranes was studied, as shown in figure 9(b). The gas selectivity of pure membrane firstly increased and then decreased gradually with increasing operation temperature. And the gas selectivities of MMM with 1 wt% filler loading reached maximum at 308 K, but gas selectivity of MMMs with 1 wt% filler loading remained a high level with increasing temperature.

The plots of gas separation performance of membranes were shown in figures 10(a) and (b). (The different color represented gas separation performance of MMMs with different loadings. The four stars were gas separation performance of MMMs with 1 wt% loadings at different temperature.) The gas separation performance of MMMs with 1 wt% filler loading was far superior to that of pure membrane. With increasing operation temperature, the gas separation performance of MMMs with 1 wt% filler loading firstly increased then decreased and reached the maximum value at 308 K.

The normalized gas selectivities for PI-based MMMs from literature were shown in figures 11(a) and (b) [54–59], normalized for the initial value of unfilled membrane. The normalized CO_2 permeability of MMMs with 1 wt% filler loading was 1.15, which was similar with the reported value [54, 56]. Compared with gas separation data from literatures, the normalized CO_2/N_2 selectivity and normalized CO_2/CH_4 selectivity in this work were both far superior to that reported. The long time operation test was shown in figure S6.

4. Conclusions

Highly porous and fast-transported MWCNT@GONRs nanohybrid was firstly used as inorganic nanofillers in MMMs with different loadings. SEM and XRD spectrum exhibited a good polymer-filler contact and a homogenous dispersion of filler throughout the polymer matrix due to the
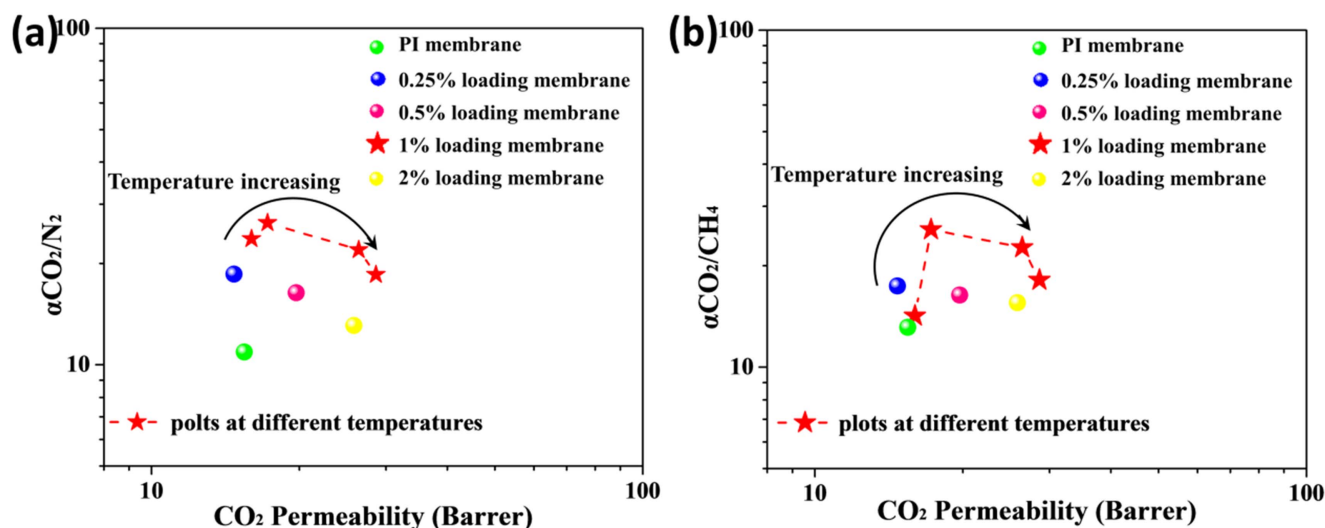
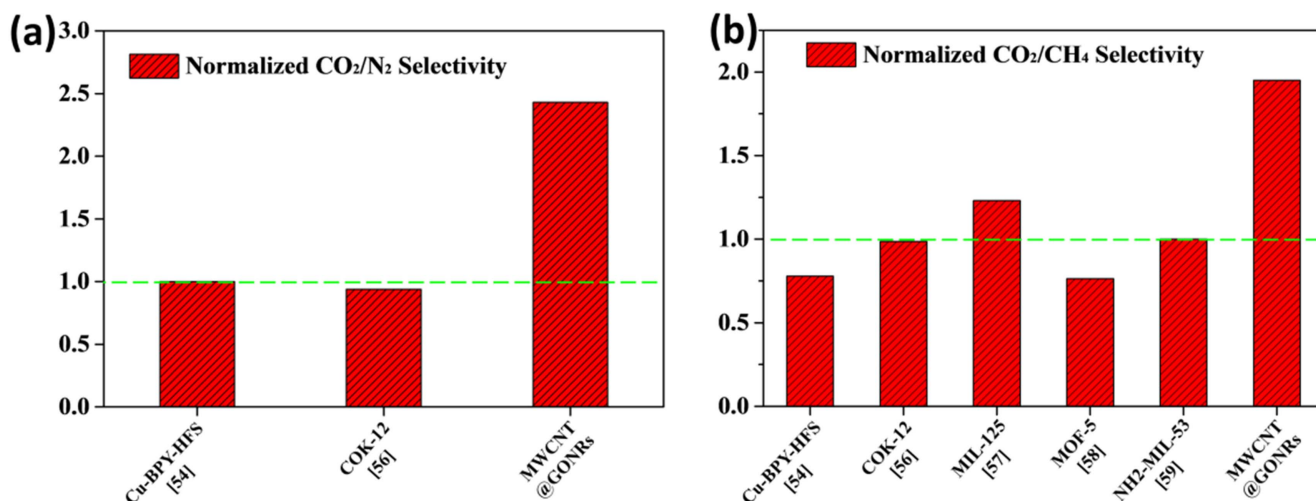**Figure 10.** Plots of CO_2/N_2 (a) and CO_2/CH_4 (b) separation performance of membranes.

Figure 11. Normalized CO_2/N_2 and CO_2/CH_4 selectivity of PI-based MMMs with different fillers.

dispersibility of GONRs shell. The measuring results showed that a low loading of core/shell MWCNT@GONRs could effectively enhance the gas separation performance of MMMs by exerting the synergistic effect of MWCNTs and GONRs. The high gas selectivity could be attributed to the GONRs shell, which provided a selective barrier and large gas adsorbed area, while the high gas permeability resulted from the hollow structured MWCNTs core with smooth internal surface, which acted as a rapid transport channels. The unique microstructures, ease of synthesis and low filling loading made MWCNT@GONRs promising candidates to improve the gas separation performance of industrial gas separation membrane.

Acknowledgments

References

[1] Cong H, Radosz M, Towler B F and Shen Y 2007 Polymer-inorganic nanocomposite membranes for gas separation *Sep. Purif. Technol.* **55** 281–91

[2] Lin H and Freeman B D 2005 Materials selection guidelines for membranes that remove CO_2 from gas mixtures *J. Mol. Struct.* **739** 57–74

[3] Aroon M A, Ismail A F, Matsuura T and Montazer-Rahmati M M 2010 Performance studies of mixed matrix membranes for gas separation: a review *Sep. Purif. Technol.* **75** 229–42

[4] Basu S, Khan A L, Cano-Odena A, Liu C and Vankelecom I F 2010 Membrane-based technologies for biogas separations *Chem. Soc. Rev.* **39** 750–68

[5] Robeson L M 1991 Correlation of separation factor versus permeability for polymeric membranes *J. Membr. Sci.* **62** 165–85

[6] Robeson L M 2008 The upper bound revisited *J. Membr. Sci.* **320** 390–400

[7] Hara N, Yoshimune M, Negishi H, Haraya K, Hara S and Yamaguchi T 2014 Diffusive separation of propylene/propane with ZIF-8 membranes *J. Membr. Sci.* **450** 215–23

[8] Liu D, Ma X, Xi H and Lin Y S 2014 Gas transport properties and propylene/propane separation characteristics of ZIF-8 membranes *J. Membr. Sci.* **451** 85–93

[9] Yilmaz G and Keskin S 2014 Molecular modeling of MOF and ZIF-filled MMMs for CO_2/N_2 separations *J. Membr. Sci.* **454** 407–17

[10] Kang Z, Peng Y, Hu Z, Qian Y, Chi C, Yeo L Y, Tee L and Zhao D 2015 Mixed matrix membranes composed of two-dimensional metal-organic framework nanosheets for pre-combustion CO_2 capture: a relationship study of filler morphology versus membrane performance *J. Mater. Chem.* A **3** 20801–10

[11] Shahid S, Nijmeijer K, Nehache S, Vankelecom I, Deratani A and Quemener D 2015 MOF-mixed matrix membranes: precise dispersion of MOF particles with better compatibility via a particle fusion approach for enhanced gas separation properties *J. Membr. Sci.* **492** 21–31

[12] Burmann P, Zornoza B, Téllez C and Coronas J 2014 Mixed matrix membranes comprising MOFs and porous silicate fillers prepared via spin coating for gas separation *Chem. Eng. Sci.* **107** 66–75

[13] Aroon M A, Ismail A F, Montazer-Rahmati M M and Matsuura T 2010 Effect of chitosan as a functionalization agent on the performance and separation properties of polyimide/multi-walled carbon nanotubes mixed matrix flat sheet membranes *J. Membr. Sci.* **364** 309–17

[14] Ansaloni L, Zhao Y, Jung B T, Ramasubramanian K, Baschetti M G and Ho W W 2015 Facilitated transport membranes containing amino-functionalized multi-walled carbon nanotubes for high-pressure CO_2 separations *J. Membr. Sci.* **490** 18–28

[15] Zhao D, Ren J, Li H, Li X and Deng M 2014 Gas separation properties of poly (amide-6-b-ethylene oxide)/amino modified multi-walled carbon nanotubes mixed matrix membranes *J. Membr. Sci.* **467** 41–7

[16] Wu B, Li X, An D, Zhao S and Wang Y 2014 Electro-casting aligned MWCNTs/polystyrene composite membranes for enhanced gas separation performance *J. Membr. Sci.* **462** 62–8

[17] Xin Q, Li Z, Li C, Wang S, Jiang Z, Wu H, Zhang Y, Yang J and Cao X 2015 Enhancing the CO_2 separation performance of composite membranes by the incorporation of amino acid-functionalized graphene oxide *J. Mater. Chem.* A **3** 6629–41

[18] Kuilla T, Bhadra S, Yao D, Kim N H, Bose S and Lee J H 2010 Recent advances in graphene based polymer composites *Prog. Polym. Sci.* **35** 1350–75

[19] Wang T, Zhao L, Shen J N, Wu L G and Van der Bruggen B 2015 Enhanced performance of polyurethane hybrid membranes for CO_2 separation by incorporating graphene oxide: the relationship between the membrane performance and the morphology of graphene oxide *Environ. Sci. Technol.* **49** 8004–11

[20] Berean K J, Ou J Z, Nour M, Field M R, Alsaif M M, Wang Y and Hill A J 2015 Enhanced gas permeation through graphene nanocomposites *J. Phys. Chem.* C **119** 13700–12

[21] Goh P S, Ismail A F, Sanip S M, Ng B C and Aziz M 2011 Recent advances of inorganic fillers in mixed matrix membrane for gas separation *Sep. Purif. Technol.* **81** 243–64

[22] Chung T S, Jiang L Y, Li Y and Kulprathipanja S 2007 Mixed matrix membranes (MMMs) comprising organic polymers with dispersed inorganic fillers for gas separation *Prog. Polym. Sci.* **32** 483–507

[23] Xin Q, Ouyang J, Liu T, Li Z, Liu Y, Wu H, Jiang Z and Cao X 2015 Enhanced interfacial interaction and CO_2 separation performance of mixed matrix membrane by incorporating polyethylenimine-decorated metal-organic frameworks *ACS Appl. Mater. Inter.* **7** 1065–77

[24] Iijima S 1991 Helical microtubules of graphitic carbon *Nature* **354** 56–8

[25] Popov V N 2004 Carbon nanotubes: properties and application *Mat. Sci. Eng.* R **43** 61–102

[26] Sholl D S and Johnson J K 2006 Making high-flux membranes with carbon nanotubes *Science* **312** 1003–4

[27] Chen H and Sholl D S 2006 Predictions of selectivity and flux for CH_4/H_2 separations using single walled carbon nanotubes as membranes *J. Membr. Sci.* **269** 152–60

[28] Holt J K, Park H G, Wang Y, Stadermann M, Artyukhin A B, Grigoropoulos C P, Noy A and Bakajin O 2006 Fast mass transport through sub-2-nanometer carbon nanotubes *Science* **312** 1034–7

[29] Zhang Z, Zhang H, Zheng Y, Wang L and Wang J 2008 Gas separation by kinked single-walled carbon nanotubes: molecular dynamics simulations *Phys. Rev.* B **78** 035439

[30] Zhang Z, Zhang H, Wang L, Ding J, Wang J, Zheng Y, Ye H, Liu Z, Cheng G and Ling Z 2011 Reassessing molecular sieving by kinked carbon nanotubes *Model Simul. Mater. Sc.* **19** 085009

[31] Skoulidas A I, Ackerman D M, Johnson J K and Sholl D S 2002 Rapid transport of gases in carbon nanotubes *Phys. Rev. Lett.* **89** 185901

[32] Qian D, Dickey E C, Andrews R and Rantell T 2000 Load transfer and deformation mechanisms in carbon nanotube-polystyrene composites *Appl. Phys. Lett.* **76** 2868–70

[33] Ismail A F, Goh P S, Sanip S M and Aziz M 2009 Transport and separation properties of carbon nanotube-mixed matrix membrane *Sep. Purif. Technol.* **70** 12–26

[34] Sahoo N G, Rana S, Cho J W, Li L and Chan S H 2010 Polymer nanocomposites based on functionalized carbon nanotubes *Prog. Polym. Sci.* **35** 837–67

[35] Guo Q, Xue Q, Sun J, Dong M, Xia F and Zhang Z 2015 Gigantic enhancement in the dielectric properties of polymer-based composites using core/shell MWCNT/amorphous carbon nanohybrids *Nanoscale* **7** 3660–7

[36] Yang D, Velamakanni A, Bozoklu G, Park S, Stoller M, Piner R D and Ruoff R S 2009 Chemical analysis of graphene oxide films after heat and chemical treatments by x-ray photoelectron and micro-Raman spectroscopy *Carbon* **47** 145–52

[37] Dreyer D R, Park S, Bielawski C W and Ruoff R S 2010 The chemistry of graphene oxide *Chem. Soc. Rev.* **39** 228–40

[38] Shan M, Xue Q, Jing N, Ling C, Zhang T, Yan Z and Zheng J 2012 Influence of chemical functionalization on the CO_2/N_2 separation performance of porous graphene membranes *Nanoscale* **4** 5477–82

[39] Zhong X, Yu H, Zhuang G, Li Q, Wang X, Zhu Y, Dong M D and Wang J G 2014 Pyridyne cycloaddition of graphene:'external' active sites for oxygen reduction reaction *J. Mater. Chem.* A **2** 897–901

[40] Jiang Z, Li J, Aslan H, Li Q, Li Y, Chen M, Dong M D and Besenbacher F 2014 A high efficiency H_2S gas sensor material: paper like Fe_2O_3/graphene nanosheets and structural alignment dependency of device efficiency *J. Mater. Chem.* A **2** 6714–7

[41] Rafiee M A, Lu W, Thomas A V, Zandiatashbar A, Rafiee J, Tour J M and Koratkar N A 2010 Graphene nanoribbon composites *ACS Nano* **4** 7415–20

[42] Kim H W *et al* 2013 Selective gas transport through few-layered graphene and graphene oxide membranes *Science* **342** 91–5

[43] Li H, Song Z, Zhang X, Huang Y, Li S, Mao Y and Yu M 2013 Ultrathin, molecular-sieving graphene oxide membranes for selective hydrogen separation *Science* **342** 95–8

[44] Yucel O, Unsal E, Harvey J, Graham M, Jones D H and Cakmak M 2015 Mechanisms of drying of graphene/poly (amide imide) solutions for films with enhanced gas barrier and mechanical as investigated by real time measurement system *J. Membr. Sci.* **495** 65–71

[45] Bandyopadhyay P, Park W B, Layek R K, Uddin M E, Kim N H, Kim H G and Lee J H 2016 Hexylamine functionalized reduced graphene oxide/polyurethane nanocomposite-coated nylon for enhanced hydrogen gas barrier film *J. Membr. Sci.* **500** 106–14

[46] Li X, Ma L, Zhang H, Wang S, Jiang Z, Guo R, Wu H, Cao X and Wang B 2015 Synergistic effect of combining carbon nanotubes and graphene oxide in mixed matrix membranes for efficient CO_2 separation *J. Membr. Sci.* **479** 1–10

[47] Zhang Z, Xue Q, Du Y, Ling C and Xing W 2014 Highly enhanced sensitivity of hydrogen sensors using novel palladium-decorated graphene nanoribbon film/SiO_2/Si structures *J. Mater. Chem.* A **2** 15931–7

[48] Higginbotham A L, Kosynkin D V, Sinitskii A, Sun Z and Tour J M 2010 Lower-defect graphene oxide nanoribbons from multiwalled carbon nanotubes *ACS Nano* **4** 2059–69

[49] Sun H, Ma C, Yuan B, Wang T, Xu Y, Xue Q and Kong Y 2014 Cardo polyimides/TiO_2 mixed matrix membranes: synthesis, characterization, and gas separation property improvement *Sep. Purif. Technol.* **122** 367–75

[50] Almadhoun M N, Hedhili M N, Odeh I N, Xavier P, Bhansali U S and Alshareef H N 2014 Influence of stacking morphology and edge nitrogen doping on the dielectric performance of graphene–polymer nanocomposites *Chem. Mater.* **26** 2856–61

[51] Wu C, Huang X, Xie L, Wu X, Yu J and Jiang P 2011 Morphology-controllable graphene–TiO_2 nanorod hybrid nanostructures for polymer composites with high dielectric performance *J. Mater. Chem.* **21** 17729–36

[52] Lin Z, Yao Y, Li Z, Liu Y, Li Z and Wong C P 2010 Solvent-assisted thermal reduction of graphite oxide *J. Phys. Chem.* C **114** 14819–25

[53] Wang X, Hu Y, Song L, Yang H, Xing W and Lu H 2011 In situ polymerization of graphene nanosheets and polyurethane with enhanced mechanical and thermal properties *J. Mater. Chem.* **21** 4222–7

[54] Zhang Y, Musselman I H, Ferraris J P and Balkus K J 2008 Gas permeability properties of Matrimid® membranes containing the metal-organic framework Cu–BPY–HFS *J. Membr. Sci.* **313** 170–81

[55] Wang S, Li X, Wu H, Tian Z, Xin Q, He G, Peng D, Jiang Z and Guiver M D 2016 Advances in high permeability polymer-based membrane materials for CO_2 separations *Energy Environ. Sci.* **9** 1863–90

[56] Khan A L, Sree S P, Martens J A, Raza M T and Vankelecom I F 2015 Mixed matrix membranes comprising of matrimid and mesoporous COK-12: preparation and gas separation properties *J. Membr. Sci.* **495** 471–8

[57] Anjum M W, Bueken B, De Vos D and Vankelecom I F 2016 MIL-125 (Ti) based mixed matrix membranes for CO_2 separation from CH_4 and N_2 *J. Membr. Sci.* **502** 21–8

[58] Perez E V, Balkus K J, Ferraris J P and Musselman I H 2009 Mixed-matrix membranes containing MOF-5 for gas separations *J. Membr. Sci.* **328** 165–73

[59] Rodenas T, van Dalen M, Serra-Crespo P, Kapteijn F and Gascon J 2014 Mixed matrix membranes based on NH_2-functionalized MIL-type MOFs: influence of structural and operational parameters on the CO_2/CH_4 separation performance *Micropor. Mesopor. Mat.* **192** 35–42